Preferential Association of Segment Blocks in Polyurethane Nanocomposites

LaShanda T. James Korley,[†,§] **Shawna M. Liff,**[‡,§] **Nitin Kumar,**[‡,§]
Gareth H. McKinley,[‡,§] **and Paula T. Hammond*,**[†,§]

Department of Chemical Engineering, Department of Mechanical Engineering, and Institute for Soldier Nanotechnologies, Massachusetts Institute of Technology, Cambridge, Massachusetts 02139

Received June 20, 2006; Revised Manuscript Received August 1, 2006

ABSTRACT: Controlling the level of dispersion of silicate layers in polymer matrices through intermolecular interactions and exploiting these interactions to enhance thermomechanical behavior are key challenges in the field of polymer nanocomposites. In this investigation, unmodified Laponite platelets are dispersed in a segmented polyurethane containing a polar, hydrophilic soft segment and a hydrophobic hard segment using a novel solvent exchange method and compared to polyurethane nanocomposites containing more hydrophobic hard and soft domains. It was determined that the silicate layers were preferentially, but not exclusively, attracted to the hydrophilic, polar soft domains. An apparent microphase-segregated morphology was observed in transmission electron microscopy for this system, revealing regions of exfoliation and intercalation. According to polarizing optical microscopy, strain-induced alignment is inhibited for this polyurethane nanocomposite, which is reflected in dramatic reductions in tensile strength and ultimate extensibility. In comparison, the Laponite disks appear to be preferentially, but not exclusively, embedded within the hard domains in the segmented polyurethanes containing more hydrophobic hard and soft domains. Exfoliation of the clay platelets leads to enhanced modulus and toughness without a reduction in extensibility. This study provides clues for exploiting silicate–polymer interactions to tune material properties without chemical modification.

Introduction

The nanoscale dispersion of layered silicates or clays in polymer matrices offers the potential for significant enhancements in material properties,[1] sparking research thrusts not only in the characterization[2,3] of these nanocomposites but also in the understanding of the thermodynamics and kinetics[4–7] governing the polymer–silicate and silicate–silicate interactions. It is well-understood that the exfoliated state, in which individual clay platelets are dispersed within a polymer matrix, maximizes polymer–clay interactions and offers the most substantial improvements in polymer properties. In the intercalated state, competing entropic and enthalpic interactions allow the polymer to be inserted within the spacing between stacked clay layers, enlarging the intergallery spacing minimally. Because the effective aspect ratio of these intercalated particle stacks is smaller than that of an individual clay platelet, the enhancements in the thermomechanical properties are less than those achieved by exfoliated silicate.[8] The majority of polymer–silicate nanocomposites developed to date exhibit intercalated morphologies due to the unfavorable interactions between the hydrophilic pristine silicate layers and the hydrophobic polymer matrix.[2] However, exfoliated morphologies have been observed in some polymer nanocomposites containing small silicate weight fractions or in polymers with low viscosities or containing strong polar groups that compete with hydrogen bonding, as in the case of nylon.[9–12] Other morphologies that can be observed in polymer–clay nanocomposites include flocculated silicate layers, which resemble the intercalated state but include edge-to-edge interactions due to the hydroxylated clay layers.[2]

Considerable efforts have been concentrated on the refinement of processing techniques, including solution and melt intercalation and in-situ polymerization, in an effort to completely exfoliate the layered silicates within the polymer matrices.[13] The hydrated cations within the galleries of pristine clay platelets render them hydrophilic and hinder the dispersion of the clay nanoparticles in often hydrophobic polymer matrices. In most methods, the hydrophilic clay surface is cation-exchanged with organophilic cations to strengthen the polymer–silicate interaction. However, the organic layer is often thermally unstable, which may lead to discoloration and a decrease in thermomechanical properties upon degradation.[14–17] Several researchers have also introduced the concept of intercalating and/or exfoliating polar silicate layers (modified or unmodified) by exploiting the relative polarity of the polymer matrix.[4–7] Yurekli and co-workers determined that in a polystyrene (PS)/poly(vinyl methyl ether) (PVME) blend, although the phase behavior was unchanged by the addition of cation-exchanged Montmorillonite, the nanoclay is preferentially associated with the more polar, PVME-rich phase in the phase-separated microstructure.[7]

Unraveling the polymer–silicate interactions becomes even more intricate when examining diblock copolymers and segmented copolymers, in which one or both blocks may exhibit significant polarity. Finnigan et al. raised the idea of using differences in block polarity in segmented polyurethanes to achieve exfoliated polyurethane/clay nanocomposites so that, in theory, exfoliation is possible through enthalpic attraction of either the hard segment or soft segment to the platelet surface, coupled with the entropic repulsion of the other block to push the layers apart.[18] Gournis and Floudas also investigated the balance of polymer–clay interactions and block–block incompatibility in poly(ethylene oxide) (PEO)–PS block copolymers and determined that multiscale levels of organization, including crystallization, microphase segregation, and intercalation, exist within the nanocomposite structure depending on clay

[†] Department of Chemical Engineering.
[‡] Department of Mechanical Engineering.
[§] Institute for Soldier Nanotechnologies.
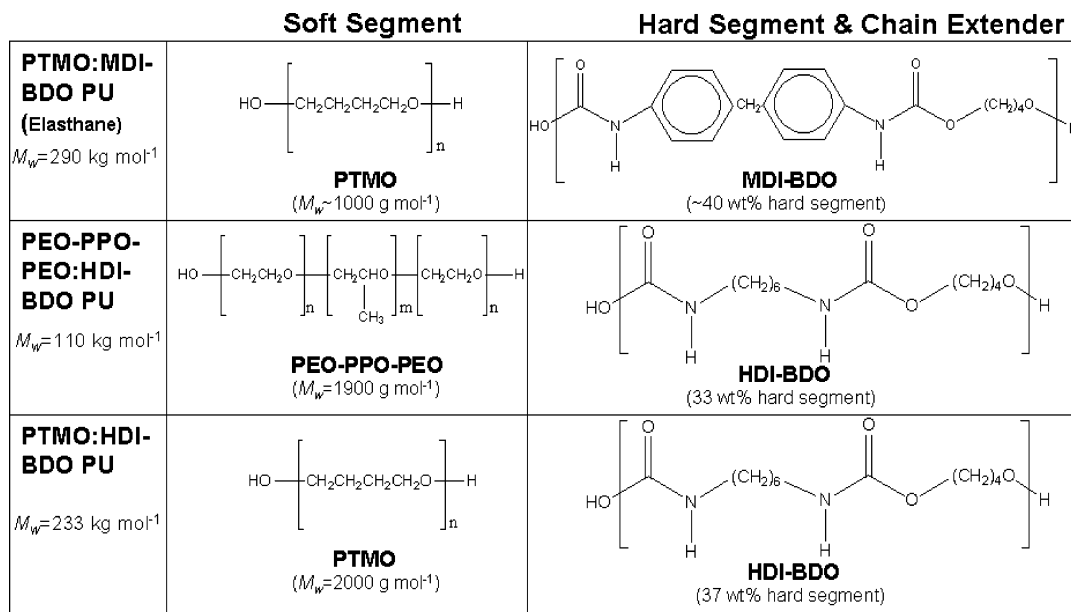[*] Corresponding author. E-mail: hammond@mit.edu.

Figure 1. Visual description of polyurethane nanocomposite matrix materials.

loading.[19] Ha et al. reported that PS-tethered Cloisite clay particles, which were exfoliated within a styrene−butadiene−styrene (SBS) block copolymer matrix and oriented using a roll-casting technique, templated the SBS morphology.[20] This clay platelet-induced morphology disrupted the alignment of the lamellar microdomains, resulting in minimal improvement in in-plane mechanical properties. Computational studies have also suggested that the microstructure and, hence, the thermomechanical properties of microphase-segregated block copolymers in polymer-layered silicate nanocomposites may be altered by exploiting segment−platelet attractions.[21,22]

In a previously studied thermoplastic polyurethane elastomer nanocomposite, Laponite RD clay disks were exfoliated within Elasthane 80A, which is composed of 4,4′-methylenebisphenyl diisocyanate−1,4-butanediol (MDI−BDO) hard segments (40 wt %) and poly(tetramethylene oxide) (PTMO) (~1000 g/mol) soft segments, using a novel solvent exchange method.[23,24] This fully exfoliated nanocomposite exhibited a dramatic 23-fold increase in initial modulus, a 50% increase in ultimate strength, and a 4-fold increase in toughness (as determined at 30% strain) at 20 wt % clay loading, without sacrificing extensibility. The results of extensive thermomechanical analysis, including an increase in heat distortion temperature (HDT) and the disappearance of a hard domain melting transition upon increased Laponite loading, indicate that the clay disks are preferentially embedded within the hard domain of the polyurethane.

The goal of this present study was to extend the development of this novel solvent exchange process to explore the influence of specific clay−polymer interactions on the mechanical behavior of segmented polyurethane (PU) elastomer-layered silicate nanocomposites containing polar, hydrophilic soft and hard segments and compare these to PU nanocomposites containing more hydrophobic hard and soft segments. This examination motivates an understanding of the level of dispersion and partitioning of unmodified clay platelets into the hard and/or soft domains and the influence of this partitioning on thermomechanical enhancement. Here, we investigate the intermolecular interactions that control dispersion (exfoliation and intercalation) and how to manipulate mechanical behavior through selective tuning of clay−polymer interactions instead of chemical modification by comparing polyurethane nanocomposites with varying degrees of polarity and hydrophilicity.

Understanding and controlling the dispersion of clay platelets into specific phases of the copolymer matrix is critical to the development of materials with unique material properties and has only been demonstrated in a few systems.[6,7,19]

Experimental Section

Materials. Two segmented polyurethane (PU) elastomers containing 1,6-hexamethylene diisocyanate−1,4-butanediol (HDI−BDO) hard segments and poly(tetramethylene oxide) (PTMO) (2000 g/mol) or poly(ethylene oxide)−poly(propylene oxide)−poly-(ethylene oxide) (PEO−PPO−PEO) (1900 g/mol; 50 wt % PEO) soft segments were synthesized using a two-step solution polymerization method. The PTMO:HDI−BDO polyurethane contained 37 wt % hard segment; the PEO−PPO−PEO:HDI−BDO polyurethane contained 33 wt % hard segment. Elasthane 80A, a soft thermoplastic polyether urethane elastomer, was provided by the Polymer Technology Group in pellet form and was used as received. The nanoclay used was Laponite RD, a synthetic, discotic, smectic clay obtained from Southern Clay Products.

Nanocomposite Formation. A well-dispersed, fully exfoliated solution of *N*,*N*-dimethylacetamide and Laponite was prepared following a previously reported solvent exchange approach.[24] In brief, this approach requires the use of two solvents, A and B, which meet four criteria: (1) solvent A fully disperses Laponite, (2) solvents A and B are fully miscible, (3) solvent A has a lower boiling point than B, and (4) the polyurethane is soluble in solvent B. For this study, solvent A was deionized water and solvent B was *N*,*N*-dimethylacetamide. The PU/nanoclay composites were then prepared by combining the *N*,*N*-dimethylacetamide and Laponite mixture with pure *N*,*N*-dimethylacetamide and 1.5 wt % polyurethane so that 0 and 10 wt % Laponite in PU films would result. The solution was heated when necessary to ensure dissolution, roll-mixed for at least 24 h, and sonicated for 1 h before slow solution casting in an oven at 60 °C with a ~0.02 m³ h⁻¹ N₂ purge. Sonication was performed as a precautionary step to ensure breakup of aggregates not visible to the naked eye. The resultant PU/nanoclay films—60 mm by 40 mm by ~0.1 mm—were then characterized.

Wide-Angle X-ray Diffraction (WAXD). X-ray diffraction was performed using a Rigaku RU300 185 mm diffractometer with an integrated germanium detector and a CuKα source with a wavelength of 1.54 Å and a scan rate of 5 °C min⁻¹.

Transmission Electron Microscopy (TEM). TEM lamellae (45 nm thickness) of PEO−PPO−PEO:HDI−BDO polyurethane nanocomposite were obtained using a RMC MT-X ultramicrotome with
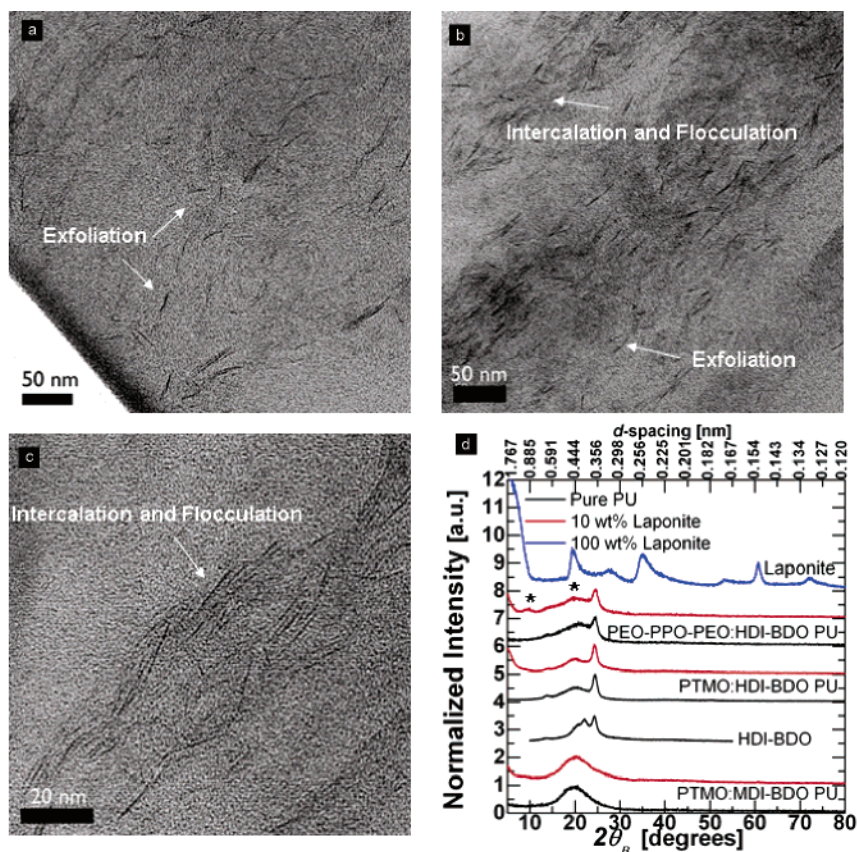
Figure 2. (a) TEM image of 10 wt % Laponite dispersed in PTMO:HDI−BDO PU; 50 nm scale bar. (b) TEM image of 10 wt % Laponite dispersed in PEO−PPO−PEO:HDI−BDO PU; 50 nm scale bar. (c) TEM image of 10 wt % Laponite dispersed in PEO−PPO−PEO:HDI−BDO PU; 20 nm scale bar. (d) WAXD data of pure Laponite and of the pure and 10 wt % Laponite-filled polyurethane nanocomposites. Also shown is a pure HDI−BDO hard segment.

CR-X cryogenic attachment. The diamond knife temperature and sample temperature were set at −95 °C and −105 °C, respectively. These cryotomed sections were then transferred to copper grids using a pig's eyelash. Unstained TEM lamellae were observed with a JEOL 2010 containing a LaB6 filament and imaged using a Gatan digital camera.

The PTMO:HDI−BDO polyurethane nanocomposite TEM lamellae were prepared in a JEOL JEM9310 focused ion beam (FIB) instrument. The samples were first sputter-coated with ∼200 nm of gold, and then a localized ∼1 μm thick carbon protective film was deposited over the area selected for lamella preparation. The samples were milled and polished in the FIB to ultimately give a lamella measuring 10 μm by 10 μm by 80 nm thick.

The PTMO:HDI−BDO PU nanocomposite lamellae were transferred to TEM grids using a micromanipulation system. The micromanipulator, a position-controlled polished glass rod, was used to pick up the lamellae (electrostatically) under an observation microscope and were then gently placed on TEM grids. These unstained TEM lamellae were observed with a JEOL 2010 containing a LaB6 filament and imaged using a Gatan digital camera.

Polarizing Optical Microscopy (POM). The long-range order, deformation, and crystalline morphologies of the PU nanocomposites before and after tensile tests were examined using a Carl Zeiss Axioskop 2MAT polarizing microscope with cross-polarized light.

Stress−Strain Experiments. Tensile tests were performed on thin-film samples approximately 60 mm by 5 mm by 0.1 mm with a 45 mm gauge length using a Zwick/Roell Z010 mechanical tester with a 500 N load cell at a constant displacement rate of 45 mm min⁻¹. At least three samples per material were tested to obtain good error estimates.

Differential Scanning Calorimetry (DSC). The soft segment glass transition temperature (T_g) and the hard segment melting temperature of the PU nanocomposites were determined via differential scanning calorimetry (DSC) using a TA Instruments Q

1000 series DSC over a temperature range of −90 to 250 °C at a ramp rate of 10 °C min⁻¹. The percent crystallinity (nonabsolute) is defined as $\Delta H_{f,HS}/\Delta H_{p,HS} \times 100$, where $\Delta H_{f,HS}$ is the enthalpy of fusion of the hard segment (J/g of hard segment) and $\Delta H_{p,HS}$ is the enthalpy of fusion of the pure hard segment (J/g of hard segment), which is 84 J/g[25] for HDI−BDO.

Dynamic Mechanical Analysis (DMA). The soft segment glass transition temperature (T_g), flexural storage modulus (E'), and the dissipation factor (tan δ) of the PU nanocomposites were determined via dynamic mechanical analysis (DMA) using a TA Instruments Q800 series DMA over a temperature range of −100 to 250 °C at a frequency of 1 Hz, a ramp rate of 3 °C min⁻¹, and an initial strain of ∼0.2%.

Results and Discussion

In this investigation, the solvent exchange method was used to disperse unmodified Laponite RD (a discotic silicate clay, 25 nm in diameter and 1 nm thick) in 1,6-hexamethylene diisocyanate−1,4-butanediol (HDI−BDO) hard segment polyurethanes containing either a poly(tetramethylene oxide) (PTMO) or poly(ethylene oxide)−poly(propylene oxide)−poly(ethylene oxide) (PEO−PPO−PEO) soft segment *without* modifying the hydrophilicity of the layered silicate. Figure 1 contains the structural details of the segmented polyurethanes for comparison.

The thermomechanical properties of these polyurethane nanocomposites are intimately related to the surface area-to-volume ratio of the nanofiller, which is a function of the level of dispersion in the polyurethane matrix. Transmission electron microscopy (TEM) and wide-angle X-ray diffraction (WAXD) provide direct evidence of the dispersed morphology of these nanocomposite materials. The TEM images (Figure 2a) of PTMO:HDI−BDO polyurethanes containing 10 wt % Laponite
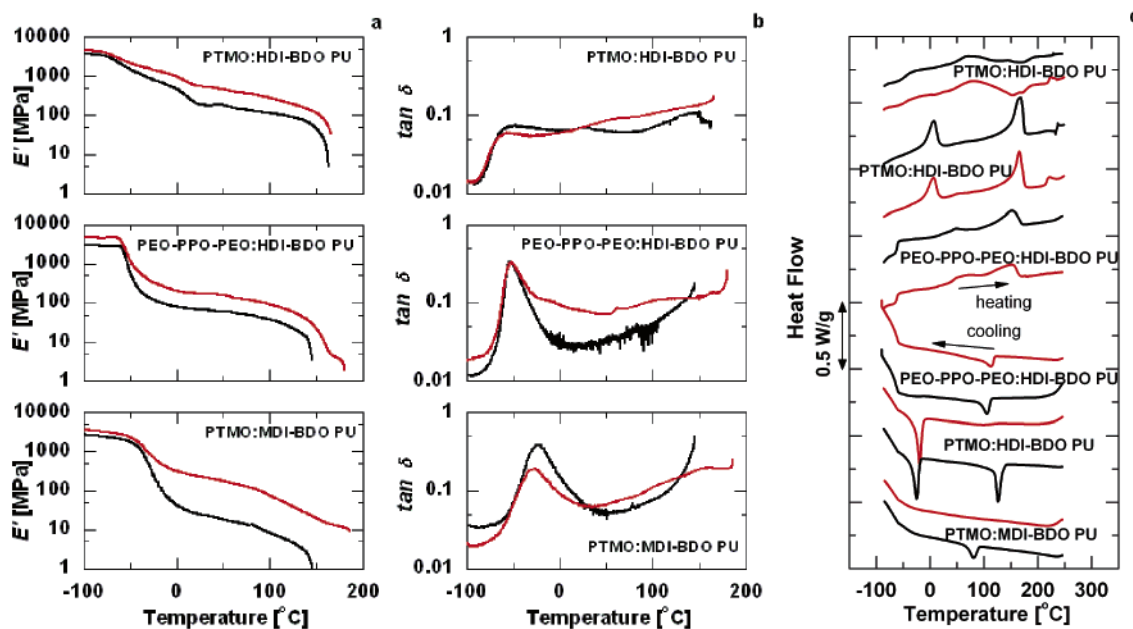
Figure 3. Flexural storage modulus, E' (a), and loss tangent, tan δ (b), both determined via DMA and DSC thermograms and (c) during initial heating and cooling cycles of the pure (black) and 10 wt % Laponite-filled PUs (red).

reveal that the clay disks are exfoliated and well-dispersed within the polyurethane matrix. In contrast, the TEM images (Figure 2b,c) of the PEO−PPO−PEO:HDI−BDO polyurethane loaded with 10 wt % Laponite highlight an apparent microphase-separated morphology, in which regions of exfoliated Laponite alternate with areas primarily populated by flocculated and intercalated structures.

Similar observations of phase separation have been reported for PEO/Montmorillonite systems above a certain PEO content and have been attributed to aggregation of clay layers to form superstructures.[26,27] Figure 2d compares the diffraction patterns ($5° \leq 2\theta \leq 80°$) of the unloaded and loaded PEO−PPO−PEO:HDI−BDO and PTMO:HDI−BDO polyurethane nanocomposites as well as the pure HDI−BDO hard segment. WAXD confirms the exfoliation of Laponite disks within the PTMO:HDI−BDO polyurethane matrix as evidenced by the lack of a detectable clay spacing diffraction peak. The WAXD patterns of PEO−PPO−PEO:HDI−BDO polyurethane nanocomposites show a broad scattering peak at $2\theta = 10°$ ($d = 0.87$ nm), which is smaller than the (001) spacing of 1.3 nm reported for pristine Laponite RD. This initially surprising result may be rationalized in terms of the well-examined intercalation of hydrophilic PEO chains into the gallery spacing of clay particles.[28−33] It appears that the observed spacing is a higher-order reflection indicative of an intercalated morphology. By calculating the first-order lamellar spacing for this proposed second-order reflection, we obtain a d-spacing of 1.78 nm ($2\theta = 4.96°$), which is consistent with the TEM image shown in Figure 2c and with the inter-calated diffraction peak found in other PEO/clay nanocom-posites.[26,29−33] On the basis of this interpretation, we assert that the observed phase-separated microstructure represents exfoli-ated hard domain-rich regions alternating with more floc-culated−intercalated soft-segment-rich regions. The typical d-spacings found for the polyurethanes range from 10 to 15 nm. The TEM images of this structure consist of striated regions, which in some areas appear wider due to overlap with under-lying domains, and the presence of the particles in the soft domain may also increase the typical sizes of the soft regions. WAXD also shows a broad peak developing at $2\theta = 18°$, which may be attributed to a PEO mesophase with $d = 4.2$ Å. This
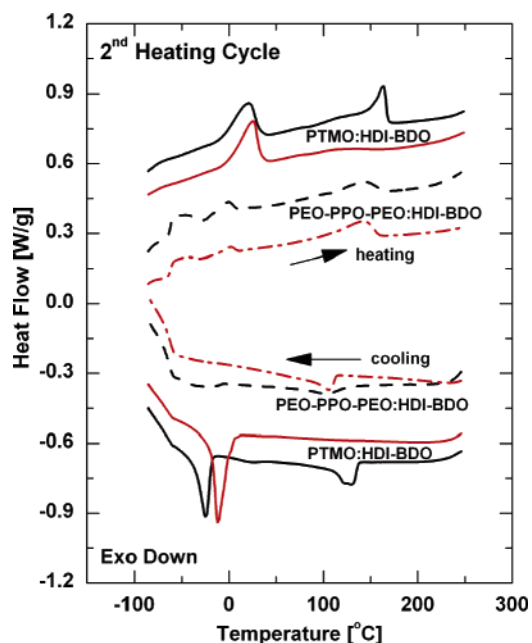

Figure 4. DSC thermograms during second heating and cooling cycles of the pure (black) and 10 wt % Laponite-filled PUs (red).

mesophase develops as a portion of the hydrophilic PEO-containing soft segments complex with the sodium ions in the gallery of the clay sheets in an extended-chain conformation.[34]

After determining the dispersed morphology of these seg-mented polyurethane elastomeric nanocomposites, the thermo-mechanical behavior of these materials was assessed using dynamic mechanical analysis (DMA) and differential scanning calorimetry (DSC), as shown in Figures 3 and 4. A comparison of the flexural storage modulus (Figure 3a) and tan δ (Figure 3b) highlights the insensitivity of the soft segment glass transition (T_g) peak positions upon addition of Laponite to the segmented polyurethane nanocomposites. However, a broaden-ing of the peak in tan δ or breadth of segmental motion at higher temperatures is observed for the PEO−PPO−PEO:HDI−BDO PU nanocomposite, providing evidence of reduced soft segment

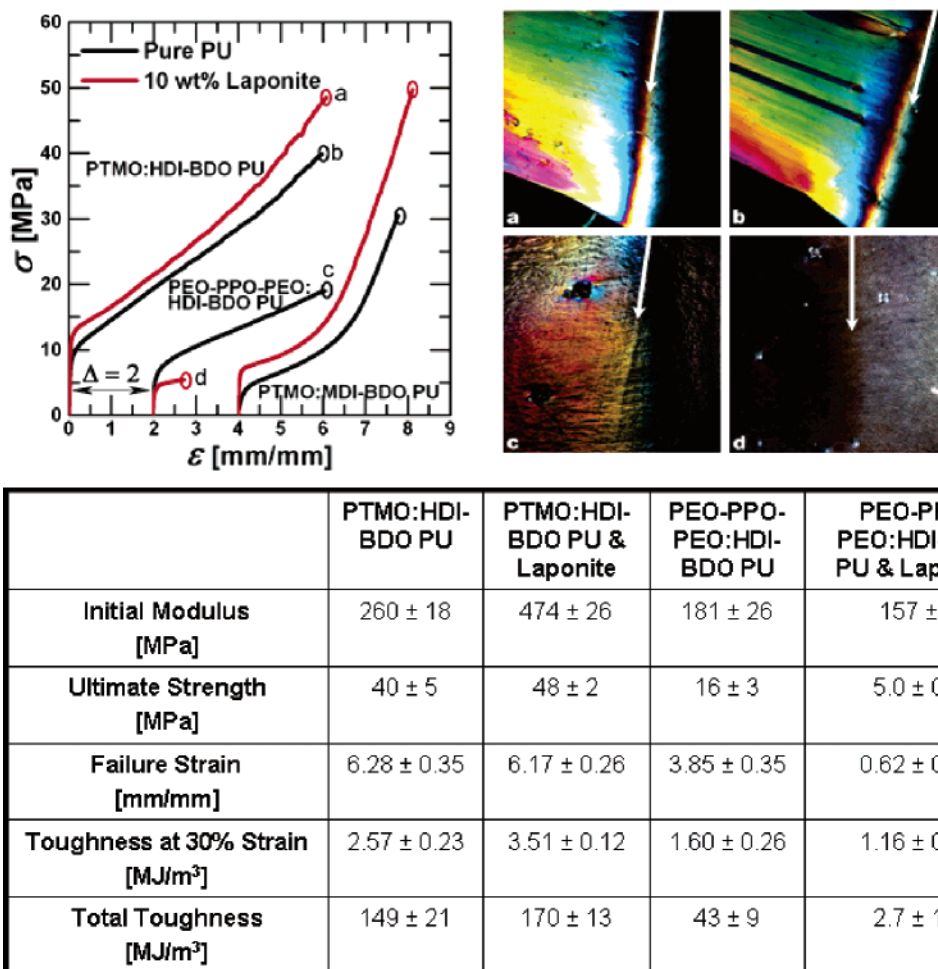|	PTMO:HDI-BDO PU	PTMO:HDI-BDO PU & Laponite	PEO-PPO-PEO:HDI-BDO PU	PEO-PPO-PEO:HDI-BDO PU & Laponite
Initial Modulus [MPa]	260 ± 18	474 ± 26	181 ± 26	157 ± 3
Ultimate Strength [MPa]	40 ± 5	48 ± 2	16 ± 3	5.0 ± 0.4
Failure Strain [mm/mm]	6.28 ± 0.35	6.17 ± 0.26	3.85 ± 0.35	0.62 ± 0.21
Toughness at 30% Strain [MJ/m³]	2.57 ± 0.23	3.51 ± 0.12	1.60 ± 0.26	1.16 ± 0.04
Total Toughness [MJ/m³]	149 ± 21	170 ± 13	43 ± 9	2.7 ± 1.1

Figure 5. Representative engineering stress−strain tensile curves of the pure and 10 wt % Laponite filled polyurethanes are presented, and the correspondingly labeled cross-polarized image (height = 2.2 mm) of four of the six samples is shown (a−d), where (a) is unfilled PTMO:HDI−BDO PU, (b) is 10 wt % Laponite filled PTMO:HDI−BDO PU, (c) is unfilled PEO−PPO−PEO:HDI−BDO PU, and (d) is 10 wt % Laponite filled PEO−PPO−PEO:HDI−BDO PU. Note the cross-polarized images of PTMO:MDI−BDO and PTMO:HDI−BDO PU thin films after deformation are similar. A white arrow runs tangent along the grip locale, separating the undeformed portion of the polyurethane (right) from the deformed portion (left) which was stretched in a direction perpendicular to the white arrow.

mobility and supporting preferential attraction of the clay particles to the highly polar PEO-based soft segment.

An examination of the first heating and cooling DSC scans (Figure 3c) provides additional clues about the specific interactions between the clay disks and the segmented polyurethanes. Here, we seek to understand the impact of the sequestering of the clay disks within the hard or soft phase on thermal behavior by examination of the soft segment glass transition and soft and hard domain melting transition. The insensitivity of the glass and melting transitions of the soft segment to clay loading in these segmented polyurethanes is confirmed by DSC data. Upon 10 wt % clay loading, the glass transition of the PTMO:MDI−BDO PU nanocomposites shifts slightly from −44.7 to −46.6 °C. A soft segment melting transition is not observed in the pure PTMO:MDI−BDO PU due to the lower molecular weight (1000 g/mol) PTMO soft segment compared to the pure PTMO:HDI−BDO PU, which has a 2000 g/mol PTMO soft segment. Laponite loading within the PTMO:HDI−BDO polyurethane matrix also initiates only a slight shift in glass transition from −63.5 to −66.2 °C, as determined from the peak in tan δ from DMA, and soft segment melting transition (6.2 °C, 31.5 J/g of soft segment to 5.5 °C, 24.7 J/g of soft segment). In the PTMO:HDI−BDO nanocomposite, re-formation of the hard domain is not observed during the first cooling curve or in subsequent heating and cooling cycles (Figure 4), despite the fast crystal-

lization kinetics[25] for HDI−BDO hard domains. Additionally, a 51% decrease in hard domain crystallinity accompanies the incorporation of silicate layers within the polyurethane matrix, suggesting that the clay particles are attracted to the polar hard domains and irreversibly disrupt their crystalline packing. This behavior is in agreement with the analogous measurements in the PTMO:MDI−BDO/Laponite nanocomposites, in which it was determined that, below a critical clay loading, the Laponite disks were preferentially embedded within the hard domains. However, this partitioning of the clay platelets into the hard domains is not absolute since a 21% reduction in soft segment crystallinity is also observed upon Laponite loading, implying moderate soft domain−Laponite interaction.

As in the PTMO:HDI−BDO and PTMO:MDI−BDO PU nanocomposites, a decrease in hard domain crystallinity (31%) is observed with addition of Laponite to the PEO−PPO−PEO: HDI−BDO polyurethane matrix. However, reversible re-formation of the hard domains (Figure 4) is observed unlike in the PTMO:HDI−BDO and PTMO:MDI−BDO PU nanocomposites, suggesting only moderate Laponite−hard domain interactions in the PEO−PPO−PEO:HDI−BDO PU nanocomposites. In fact, the percent crystallinity of the hard domain is essentially constant between the first and second heating cycles, 61.0% and 58.6%, respectively, after Laponite loading. Although the soft segment melting transition is obscured in the first heating

cycle, a weak melting transition for the soft domain is observed during the second heating cycle (Figure 4) of the pure (−2.8 °C, 7.2 J/g of soft segment) and 10 wt % Laponite-loaded (−0.5 °C, 3.1 J/g of soft segment) PEO−PPO−PEO:HDI−BDO polyurethanes. The chosen cooling rate (10 °C min⁻¹) may have masked the crystallization peak of this weak transition. One explanation for the 57% reduction in soft segment crystallinity is the disruption of crystalline packing of the soft segment chains due to the favorable Laponite−PEO interaction. The soft segment T_g of the PEO−PPO−PEO:HDI−BDO PU nanocomposite remains unchanged (−61.5 to −61.7 °C) as in the PTMO: HDI−BDO and PTMO:MDI−BDO PU nanocomposites. It is likely that only a fraction of PEO−PPO−PEO resides within the Laponite galleries; the unbound soft segment dominates the thermal behavior of the nanocomposite due to the inaccessibility of the thermal dissociation temperature of the Laponite/PEO− PPO−PEO interactions.

The consequences of this morphology are reflected in the tensile properties of the PEO−PPO PEO:HDI−BDO polyurethane/clay nanocomposite, as shown in Figure 5. In contrast to the PTMO:MDI−BDO PU nanocomposite at 10 wt % clay loading, the PEO−PPO−PEO:HDI−BDO nanocomposite displays a substantial reduction in toughness (∼16-fold), ultimate tensile strength (∼3-fold), and elongation (∼6-fold). However, the initial modulus, which is usually attributed to the hard domain rigidity, remains relatively constant at this Laponite loading. The lack of birefringence in POM (Figure 5d) in the deformed regions of the PEO-based polyurethane nanocomposite further supports these tensile measurements, indicating the suppression of strain-induced alignment and the inhibition of strain-induced crystallinity in the soft segment that is evident in the pure PEO−PPO−PEO:HDI−BDO polyurethane (Figure 5c). Here, it appears that the presence of silicate layers that preferentially reside in the soft segment can limit the native ordering mechanisms that take place in the polyether upon deformations higher than 100−200%. Although not as dramatically improved as the PTMO:MDI−BDO PU nanocomposite, the PTMO:HDI−BDO polyurethane nanocomposite shows an increase in toughness (∼15%), initial modulus (2-fold increase), and ultimate strength (∼20%), while maintaining flexibility. The improvement in initial modulus, which is usually attributed to hard domain rigidity, also supports the model of Laponite disks preferentially associated within the HDI−BDO hard domains. One possible explanation for the moderate thermomechanical enhancement compared to the PTMO:MDI−BDO PU nanocomposite is that, while the Laponite disks in the PTMO:HDI− BDO PU nanocomposites are primarily sequestered in the hard domain and that these intermolecular interactions dominate the level of dispersion, and, hence mechanical behavior, a portion of the clay platelets are also interacting with soft domains, as suggested by the decrease in soft segment crystallinity (DSC). As in the PTMO:MDI−BDO PU nanocomposite (Figure 5a), POM images of the PTMO:HDI−BDO PU nanocomposite (Figure 5b) detail the strain-induced birefringence indicative of soft segment alignment during the deformation process.

Conclusions

In this research, a novel solvent exchange method has allowed the *primarily exfoliated* dispersion of unmodified clay platelets into an elastomeric polyurethane matrix containing a polar hard block and polar, hydrophilic soft block (PEO−PPO−PEO). This investigation of unmodified clay/polyurethane nanocomposites extends the wealth of literature addressing the complex behavior of PEO and PEO−PPO−PEO when intercalated and/or exfoliated with unmodified Laponite. Thermomechanical and mor-

phological behavior were explored to confirm the preferred interactions between the polyurethane blocks and the layered silicates. The hydrophilic, polar soft block (PEO−PPO−PEO) dominated the clay−polyurethane interactions in the PEO− PPO−PEO:HDI−BDO nanocomposites. POM suggests that strain-induced alignment of the soft segment chains is suppressed within the nanocomposite, which resulted in a substantial reduction in toughness and extensibility. By comparison, the silicate layers in segmented polyurethanes containing a hydrophobic soft block (PTMO) and MDI−BDO or HDI−BDO hard domains were preferentially embedded within the hard block, enhancing toughness and initial modulus, while preserving the elastomeric nature of the materials. These observations may serve as guides in the selective tailoring of the properties of polyurethane nanocomposites for a variety of applications by moderating the clay/segment interactions through calculated material design.

References and Notes

(1) Pinnavaia, T. J.; Beall, G. W. *Polymer-Clay Nanocomposites;* Wiley: New York, 2000.
(2) Ray, S. S.; Okamoto, M. *Prog. Polym. Sci.* **2003**, *28*, 1539−1641.
(3) Thostenson, E. T.; Li, C.; Chou, T.-W. *Compos. Sci. Technol.* **2005**, *65*, 491−516.
(4) Vaia, R. A.; Giannelis, E. P. *Macromolecules* **1997**, *30*, 8000−8009.
(5) Vaia, R. A.; Giannelis, E. P. *Macromolecules* **1997**, *30*, 7990−7999.
(6) Hou, S.-S.; Bonagamba, T. J.; Beyer, F. L.; Madison, P. H.; Schmidt-Rohr, K. *Macromolecules* **2003**, *36*, 2769−2776.
(7) Yurekli, K.; Karim, A.; Amis, E. J.; Krishnamoorti, R. *Macromolecules* **2004**, *37*, 507−515.
(8) Sheng, N.; Boyce, M. C.; Parks, D. M.; Rutledge, G. C.; Abes, J. I.; Cohen, R. E. *Polymer* **2004**, *45*, 487−506.
(9) Chen, T. K.; Tien, Y. I.; Wei, K. H. *Polymer* **2000**, *41*, 1345−1353.
(10) Okada, A.; Kawasumi, M.; Usuki, A.; Kojima, Y.; Kurauchi, T.; Kamigaito, O. In *Synthesis and Properties of Nylon-6/Clay Hybrids*; *MRS Symp. Proc.* **1990**, 45−50.
(11) Tien, Y. I.; Wei, K. H. *J. Appl. Polym. Sci.* **2002**, *86*, 1741−1748.
(12) Tortora, M.; Gorrasi, G.; Vittoria, V.; Galli, G.; Ritrovati, S.; Chiellini, E. *Polymer* **2002**, *43*, 6147−6157.
(13) Krishnamoorti, R.; Vaia, R. A. *Polymer Nanocomposites: Synthesis, Characterization, and Modeling*; *ACS Symp. Ser.* **2002**, *804*.
(14) VanderHart, D. L.; Asano, A.; Gilman, J. W. *Chem. Mater.* **2001**, *13*, 3781−3795.
(15) Xie, W.; Xie, R. C.; Pan, W. P.; Hunter, D.; Koene, B.; Tan, L. S.; Vaia, R. A. *Chem. Mater.* **2002**, *14*, 4837−4845.
(16) Fornes, T. D.; Yoon, P. J.; Paul, D. R. *Polymer* **2003**, *44*, 7545−7556.
(17) Dharaiya, D.; Jana, S. C. *Polymer* **2005**, *46*, 10139−10147.
(18) Finnigan, B.; Martin, D.; Halley, P.; Truss, R.; Campbell, K. *Polymer* **2004**, *45*, 2249−2260.
(19) Gournis, D.; Floudas, G. *Chem. Mater.* **2004**, *16*, 1686−1692.
(20) Ha, Y.-H.; Kwon, Y.; Breiner, T.; Chan, E. P.; Tzianetopoulou, T.; Cohen, R. E.; Boyce, M. C.; Thomas, E. L. *Macromolecules* **2005**, *38*, 5170−5179.
(21) Balazs, A. C.; Singh, C.; Zhulina, E. *Macromolecules* **1998**, *31*, 8370−8381.
(22) Balazs, A. C.; Ginzburg, V. V.; Qiu, F.; Peng, G.; Jasnow, D. *J. Phys. Chem. B* **2000**, *104*, 3411−3422.

(23) Liff, S. M.; Kumar, N.; McKinley, G. H. Submitted for publication in *Nat. Mater*.

(24) Kumar, N.; Liff, S. M.; McKinley, G. H. Method to disperse and exfoliate nanoparticles. US Patent Application, 11/253,219, Oct 18, 2005.

(25) Li, Y.; Ren, Z. Y.; Zhao, M.; Yang, H.; Chu, B. *Macromolecules* **1993**, *26*, 612−622.

(26) Kurian, M.; Galvin, M. E.; Trapa, P. E.; Sadoway, D. R.; Mayes, A. M. *Electrochim. Acta* **2005**, *50*, 2125−2134.

(27) Ogata, N.; Kawakage, S.; Ogihara, T. *Polymer* **1997**, *38*, 5115.

(28) Aranda, P.; Ruiz-Hitzky, E. *Chem. Mater*. **1992**, *4*, 1395−1403.

(29) Aranda, P.; Ruiz-Hitzky, E. *Acta Polym*. **1994**, *45*, 59.

(30) Aranda, P.; Ruiz-Hitzky, E. *Appl. Clay Sci*. **1999**, *15*, 119.

(31) Ruiz-Hitzky, E.; Aranda, P. *Adv. Mater*. **1990**, *2*, 545.

(32) Vaia, R. A.; Vasudevan, S.; Krawiec, W.; Scanlon, L. G.; Giannelis, E. P. *Adv. Mater*. **1995**, *7*, 154.

(33) Wu, J. H.; Lerner, M. M. *Chem. Mater*. **1993**, *5*, 835−838.

(34) Zukalova, M.; Rathousky, J.; Zukal, A. *Collect. Czech. Chem. Commun*. **2003**, *68*, 2019−2031.